DAEHAN HWAHAK HWOEJEE
(*Journal of the Korean Chemical Society*)
Vol. 23, No. 4, 1979
Printed in the Republic of Korea

초소성변형의 분자론

金昌弘* · 李泰圭
한국과학원 화학과

(1979. 5. 23 접수)

Molecular Theory of Superplastic Deformation

Chang Hong Kim* and **Taikyue Ree**
Department of Chemistry, Korea Advanced Institute of Science, Seoul, Korea

(Received May 23, 1979)

요 약. 소성변형에 대한 著者들의 이론을 초소성합금(Zn-Al eutectoid, Al-Cu, Pb-Sn, Sn-Bi, Mg-Al eutectics)에 적용하였다. 그 결과 초소성합금의 소성변형은 두 개의 grain boundary 流動單位의 平行連結로 나타낼 수 있었다.

이 두 개의 流動單位는 流動式에 나타나는 parameter X_{gj}/α_{gj}와 β_{gj}(j=1 혹은 2)로 表現할 수 있으며 이들을 實驗的으로 求할 수 있었다. 著者들의 流動式은 實驗과 잘 一致하였다. Strain rate sensitivity 對 -ln(strain rate) 곡선을 이론으로 구한 결과 유동단위수만큼의 peak가 β_{gj}(j=1 or 2) 값에 따라 분리되어 나타났고 초소성의 조건도 β_{gj} 값에 의하여 결정됨을 알았다. β_{gj} 값의 粒子크기 依存性을 구하였고 온도변화에 따른 β_{gj} 값 변화로부터 각 流動單位의 활성화엔탈피, ΔH^*_{gj}도 구하였다. 그 결과 ΔH^*_{gj}는 재료성분원소들의 grain boundary 자체확산에 의한 활성화엔탈피와 같이 나타났고 또 이들은 粒子 크기 증가에 따라 증가함을 보였다.

ABSTRACT. The authors' theory for plastic deformation was applied to superplastic alloys (Zn-Al eutectoid, Al-Cu, Pb-Sn, Sn-Bi, Mg-Al eutectics). The plastic deformation of the superplastic alloys could be described by two Maxwell models connected in parallel which represent two grain boundary flow units. The flow units are characterized by the two parameters X_{gj}/α_{gj} and β_{gj} (j=1 or 2, g signifies the grain boundary) the values of which were obtained by applying our flow equation [Eq. (5)] to experiment. We confirmed that our flow equation describes the superplasticity very well.

The curve of strain rate sensitivity m ($=\partial \ln f/\partial \ln \dot{s}$) *vs.* $-\ln \dot{s}$, where f and $\dot{s}$ are stress and strain rate, respectively, showed two peaks corresponding to flow unit g1 and g2, the separation of the two peaks is determined by the difference between β_{g1} and β_{g2}. The condition of superplasticity is also determined by β_{gj}, which satisfies $\dot{s}_{mj} \leqslant 1.53/\beta_{gj}$ [Eq. (13)], where $\dot{s}_{mj}$ is the $\dot{s}$ of the jth unit at the peak. The grain size dependence of β_{gj} is described by $\ln(\beta_{gj})^{-1}=a\ln x+b$ [Eq. (16)], where x is the grain size, and a and b are constants. The activation enthalpy for each flow unit, ΔH^*_{gj}, was also determined from the temperature dependence of β_{gj} which is proportional to the relaxation time of the j th unit. Since the superplasticity is determined by

*Present address: Korea Institute of Science and Technology, Seoul, Korea

Eq. (13), and since β_{gj} and ΔH_{gj}^{*} are related, we obtained the conclusion that superplasticity occurs in the system having small ΔH_{gj}^{*} values. The ΔH_{gj}^{*} values were equal to the activation enthalpies of grain boundary self-diffusion of the component atoms of the alloys, this accords with our proposed flow mechanism. The ΔH_{gj}^{*} value increases with grain size as expected from Eq. (16).

INTRODUCTION

Superplastic phenomena of alloys of exceptionally large elongation(>1000 %) without necking have been of interest for the two reasons: first, there have been proposed in the literatures (see below) various possible mechanisms for the deformation processes, but none of them is satisfactory; second, superplastic alloys have good formability like polymer melts and glasses, so these materials have possibilities for many industrial applications.

Although Pearson[1] found 1950 % tensile deformation of Sn-Bi alloy in 1934, this sensational result was ignored for 30 years until Underwood[2] and Backofen[3] started systematic studies for superplastity.

The superplastic phenomena have the following characteristics: (1) superplasticity appears in the middle range (region II) with the highest slope in the plot of $\ln f$ (f=stress) *vs.* $\ln \dot{s}$ ($\dot{s}$= strain rate) which has three different regions (I, II, and III) of different slopes; (2) the materials, in general, have fine-grained crystallographic structure;[4] and (3) after large elongation, the grain structure remains in almost equiaxial state, and many metallographic observations show prominent grain boundary sliding.[4] The phenomena usually appear over the range of temperatures where recovery or recrystallization occurs.

The representative mechanisms so far proposed are diffusional creep on grain boundaries[5] and grain boundary sliding with diffusional accommodation.[6] The above mechanisms are successful in some degree in explaining only the deformation occurring in region II, but they fail beyond region II, *i.e.*, in regions I and III. Kim and Ree[7] proposed a theory of plastic deformation which explains successfully the deformation of solids in a wide range of f and $\dot{s}$. In this paper, the Kim-Ree theory will be briefly reviewed, and it will be applied to superplastic deformation in order to see whether the theory is successful in all ranges of plastic deformation.

THEORY

1. Relations between Shear Stress and Strain Rate

According to Kim-Ree's theory,[7] plastic deformation of solids occurs by dislocation movement and/or grain boundary movement. They proposed the following mechanical model which are depicted in *Fig.* 1: (1) there are i

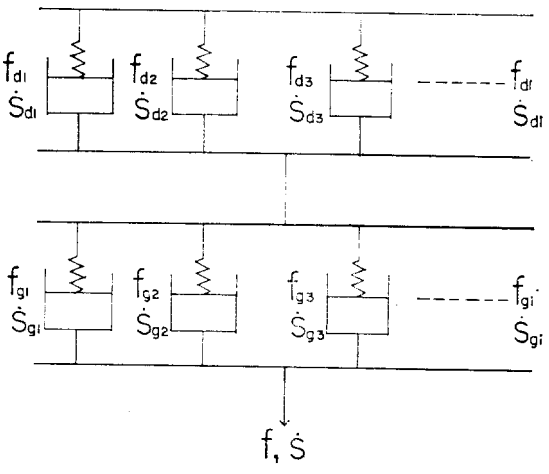

Fig. 1. Mechanical model for plastic deformation. The dislocation flow units di (i=1, 2, *etc.*) are connected in parallel, and the grain boundary flow units gj (j=1, 2, *etc.*) are also connected in parallel. The di and gj systems are connected in series.

Maxwell flow units of dislocation movement on a dislocation shear plane, and j Maxwell flow units of grain boundary movement on a grain boundary shear plane; (2) the i flow units of dislocation are connected in parallel with each other, and the j flow units of grain boundary movement are also connected in parallel; but (3) the two types of flow units, which are located on different shear planes, are connected in series as shown in ***Fig.*** 1. With this model, we obtained for stress (f), the following relations:

$$f=f_d=f_g=\sum_i \frac{X_{di}}{\alpha_{di}}\sinh^{-1}\beta_{di}\dot{s}_d$$
$$=\sum_j \frac{X_{gj}}{\alpha_{gj}}\sinh^{-1}\beta_{gj}\dot{s}_g \qquad (1)$$

and for strain rate ($\dot{s}$):

$$\dot{s}=\dot{s}_d+\dot{s}_g=\frac{1}{\beta_{di}}\sinh\alpha_{di}f_{di}$$
$$+\frac{1}{\beta_{gj}}\sinh\alpha_{gj}f_{gj} \qquad (2a)$$

where subscripts d and g represent dislocation and grain boundary movement, respectively. In Eq. (1) and (2a),

$$\alpha_{km}=\left(\frac{\lambda\lambda_2\lambda_3}{2kT}\right)_{km} \qquad (2b)$$

and

$$\beta_{km}=\left(\frac{\lambda}{\lambda_1}2k'\right)^{-1}_{km} \qquad (2c)$$

where $k=d$ or g and $m=i$ or j, λ, λ_2, λ_3 are the molecular parameters in Eyring's theory of flow,[8] k' is the frequency of a flow unit for jumping from an equilibrium position to the next equilibrium position, and X_{km} represents the fraction of the area occupied by the mth flow unit of flow type k on shear plane k. Considering the phenomenological characteristics described in the Introduction, superplasticity is related to the grain boundary movement. So if the contribution of dislocation movement is neglected, the plastic deformation can be described as the grain boundary movement only, and the general flow Eqs. (1) and (2a) can be transformed into the following equations:

$$f=f_g=\sum_j \frac{X_{gj}}{\alpha_{gj}}\sinh^{-1}\beta_{gj}\dot{s}_g \qquad (3)$$

and

$$\dot{s}=\dot{s}_g=\frac{1}{\beta_{gj}}\sinh\alpha_{gj}f_{gj} \qquad (4)$$

Equations (3) and (4) belong to the plastic deformation of Case 2 according to Kim and Ree's theory.[7] For the system composed of two kinds of grain boundary flow units, Eqs. (3) and (4) are transformed into the following equations:

$$f=\frac{X_{g1}}{\alpha_{g1}}\sinh^{-1}\beta_{g1}\dot{s}+\frac{X_{g2}}{\alpha_{g2}}\sinh^{-1}\beta_{g2}\dot{s} \qquad (5a)$$

and

$$\dot{s}=\dot{s}_{g1}=\dot{s}_{g2}=\frac{1}{\beta_{g1}}\sinh\alpha_{g1}f_{g1}$$
$$=\frac{1}{\beta_{g2}}\sinh\alpha_{g2}f_{g2} \qquad (5b)$$

Since the two flow units $g1$ and $g2$ are on the same shear plane and are connected in parallel mechanically, the shear rates of the two flow units are equal (*i.e.*, $\dot{s}_{g1}=\dot{s}_{g2}=\dot{s}$) as shown in Eq. (5b), and the total stress of the system is equal to the sum of stresses applied on each flow units (*i.e.*, $f=X_{g1}f_{g1}+X_{g2}f_{g2}$) as expressed by Eq. (5a). By applying Eq. (5a) to an experimental flow curve of f *vs.* $\dot{s}$, we can determine the parametric values of X_{gj}/α_{gj} and β_{gj} ($j=1$ or 2). For the method for determining the flow parameters, reference is made to Kim and Ree's paper.[7]

Now let us consider the molecular view point of the grain boundary movement. On grain boundary surfaces, there are many obstacles so called "the bad sites,"[7] such as ledges,[5]

bumps,[4] precipitates,[9] impurities,[9] and grain boundary dislocations.[9] Whenever a bad site on a grain (called grain A) encounters a bad site on grain B on a shear surface, the movement of grain A is impeded, thus the applied stress is concentrated on the bad sites in contact as well as on the neighboring atoms. As a result, the atoms diffuse away along the grain boundary in order to release the stress. When sufficient self-diffusion occurred, the movement of grain A is possible. Thus, the bad site on grain A is considered to be the flow unit represented by a Maxwellian model previously mentioned. If two kinds of atoms are neighbored near the bad sites(as in the case of binary alloys), there will be two kinds of self-diffusion processes for grain boundary movement, and the movement requires two kinds of activation energies for the two flow units. Examples of superplastic materials are usually eutectics or eutectoids, which are all binary alloys, and have fine-grained structures. So, for the plastic deformation of these alloys, one can expect that the contribution of grain boundary movement is predominant, and the flow behavior can be adequately described by Eq. (5a).

2. Strain Rate Sensitivity

Strain rate sensitivity m is defined as

$$m=\frac{d\ln f}{d\ln \dot{s}} \tag{6}$$

When $m=1$, the flow is Newtonian; and when $m\geq 0.3$, the tendency of superplasticity appears without necking.[3] Usually alloys have the value of $m=0.02$ to 0.2, polymers have $m=0.3$ to 1.0, and superplastic alloys have $m=0.3$ to 0.9. To obtain the value of m theoretically from the authors' flow equation, Eq. (3) is differentiated with respect to $\dot{s}$ as shown below:

$$df=\sum_j \frac{X_{gj}}{\alpha_{gj}} \frac{\beta_{gj}\dot{s}}{[1+(\beta_{gj}\dot{s})^2]^{1/2}} \frac{d\dot{s}}{\dot{s}} \tag{7}$$

By a simple manipulation, Eq. (7) is transformed into:

$$\frac{d\ln f}{d\ln \dot{s}}\equiv m=\frac{1}{f}\sum_j \frac{X_{gj}}{\alpha_{gj}} \frac{\beta_{gj}\dot{s}}{[1+(\beta_{gj}\dot{s})^2]^{1/2}} =\sum m_j \tag{8}$$

Here m_j represents the strain rate sensitivity of the jth flow unit, and is defined as

$$m_j=\frac{1}{f}\frac{X_{gj}}{\alpha_{gj}} \frac{\beta_{gj}\dot{s}}{[1+(\beta_{gj}\dot{s})^2]^{1/2}} \tag{9}$$

The schematic curve of Eq. (8) for the system of two flow units connected in parallel are shown in *Fig.* 2. Two peaks appear separately, each corresponding to flow unit 1 and 2, respectively. If the values of β_{gj} are different enough in magnitude, the curve of m would have maxima equal to the number of flow units in the system. The flow unit of the largest β_{gj} value would have a maximum at the lowest $\dot{s}$, and as β_{gj} value decreases, the maximum appears at higher $\dot{s}$ with a smaller maximum value of m. Thus the total strain rate sensitivity curve would show a band spectrum, each band corresponding to each flow unit.

The β_{gj}^{-1} defined by Eq. (2c) can be expressed[7] by the following equation:

$$\beta_{gj}^{-1}=\left(\frac{\lambda}{\lambda_1}\right)_{gj}\frac{2kT}{h}\exp\left(\frac{\Delta S_{gj}^{*}}{R}\right) \cdot \exp\left(\frac{-\Delta H_{gj}^{*}}{RT}\right) \tag{10}$$

where ΔH_{gj}^{*} and ΔS_{gj}^{*} are the activation enthalpy and activation entropy for the jumping process, respectively.

From Eq. (9) in conjunction with the condition of $dm_1/d\dot{s}=0$ at the maximum point of m for flow unit 1 where $\dot{s}=\dot{s}_{m1}$ and $f=f_{m1}$ (see *Fig.* 2), the following equation is obtained:

$$\left(\frac{dm_1}{d\dot{s}}\right)_{\dot{s}_{m1}}=\frac{1}{1+(\beta_{g1}\dot{s}_{m1})^2}-\left(\sum_j m_j\right)_{\dot{s}_{m1}}=0 \tag{11a}$$

Next, it is assumed that at the maximum point, the contributions of other flow units to m is negligible compared to unit 1, *i.e.*

$$\left(\sum_j m_j\right)_{\dot{s}_{m1}}\approx(m_1)_{\dot{s}_{m1}} \tag{11b}$$

Thus we obtain from Eqs. (11a) and (11b),

$$\frac{1}{1+(\beta_{g1}\dot{s})^2}\approx(m_1)_{\dot{s}_{m1}}=\frac{1}{f_{m1}}\cdot\frac{X_{g1}}{\alpha_{g1}}\cdot\frac{\beta_{g1}\dot{s}_{m1}}{[1+(\beta_{g1}\dot{s}_{m1})^2]^{1/2}} \tag{11c}$$

where the second equality of Eq. (11c) was obtained by using Eq. (9) [where $j=1$, $f=f_{m1}$ and $\dot{s}=\dot{s}_{m1}$]. From Eq. (11c), the following results:

$$\frac{1}{f_{m1}}\frac{X_{g1}}{\alpha_{g1}}\approx\frac{1}{[1+(\beta_{g1}\dot{s}_{m1})^2]^{1/2}}\cdot\frac{1}{\beta_{g1}\dot{s}_{m1}}=\frac{X_{g1}}{\alpha_{g1}}\cdot\frac{1}{\frac{X_{g1}}{\alpha_{g1}}\sinh^{-1}(\beta_{g1}\dot{s}_{m1})+\frac{X_{g2}}{\alpha_{g2}}\sinh^{-1}(\beta_{g2}\dot{s}_{m1})} \tag{11d}$$

where the second equality was obtained by introducing Eq. (5a) (with $\dot{s}=\dot{s}_{m1}$) to f_{m1} on the left of the first equality of Eq. (11d). The $\dot{s}_{m1}$ satisfying Eq. (11d) can be obtained by numerical calculation if the flow parameters are given. The maximum value $m_1(\max.)$ can be calculated by Eq. (11c):

$$m_1(\max.)=\frac{1}{f_{m1}}\frac{X_{g1}}{\alpha_{g1}}\frac{\beta_{g1}\dot{s}_{m1}}{[1+(\beta_{g1}\dot{s}_{m1})^2]^{1/2}}=\frac{1}{1+(\beta_{g1}\dot{s}_{m1})^2} \tag{12}$$

where the first equality of Eq. (11d) has been substituted for $X_{g1}/(\alpha_{g1}f_{m1})$. If Eq. (12) satisfies the condition, $m_1(\max.)\geqslant 0.3$, this system (or material) would have at least a superplastic region. From this condition, the following simple relation is obtained:

$$m_1(\max.)=\frac{1}{1+(\beta_{g1}\dot{s}_{m1})^2}\geqslant 0.3$$

and

$$\dot{s}_{m1}\leqslant\frac{1.53}{\beta_{g1}} \tag{13}$$

That is, if $\dot{s}_{m1}$ in Eq. (11d) satisfies the inequality (13), the material can be considered to have a superplastic region. The inequality (13) shows also that as β_{gj} increases the maximum point shifts to lower strain rate region. Therefore, superplasticity can be considered to be a property of materials determined by temperature, activation enthalpy and grain size (see below). Moreover, one may see that by controlling the properties of materials and working conditions (*i.e.*, by controlling β_{gj} values), the superplastic region favorable to industrial operation can be selected theoretically. Thus promising contributions of our theory to industry are expected.

3. Calculation of Activation Enthalpies.

According to Eq. (10), β_{gj}^{-1} is a function of temperature, activation enthalpy and activation entropy, and the activation enthalpy is also a function of grain size (see below). If the grain size and activation entropy are constant, the temperature dependence of β_{gj}^{-1} can be expressed as [see Eq. (10)]

$$\ln\beta_{gj}^{-1}=\frac{-\Delta H_{gj}^{*}}{R}\frac{1}{T}+A_{gj} \tag{14}$$

where A_{gj} is a constant for a given grain size. The plot of $\ln\beta_{gj}^{-1}$ *vs.* $1/T$ yields a straight line whose slope and intercept are $-\Delta H_{gj}^{*}/R$ and A_{gj}, respectively. From the slope, the activation enthalpy of the gj flow unit, ΔH_{gj}^{*}, can be obtained. Experimentally, the straight line was drawn by least square fit of the plot of $\ln\beta_{gj}^{-1}$ *vs.* $1/T$.

Superplastic materials are commonly found in binary eutectics and eutectoid alloys. After analysing the flow curves, we found two activation enthalpies (see below). As previously

mentioned, the two activation enthalpies mean that for binary eutectics and eutectoid alloys, two kinds of atoms around obstacles would diffuse away along the grain boundary. It is also noted from Eq. (13) that the material with small β_{gj} would show superplasticity in general.

4. Grain Size Dependence of β

Let us examine the dependence of β_{gj}^{-1} on grain size. Referring to Eq. (10), λ_1 and λ are values of the same order of magnitude of atomic or grain sizes. If the grain size increases, λ_1 and λ will also increase in the same proportion, hence the ratio λ/λ_1 would be independent on the grain size. If we assume that the activation entropy change with grain size is negligible, the activation enthalpy becomes to be a function of grain size. In actual cases, the slope of the curve $\ln \beta_{gj}^{-1}$ *vs.* $1/T$ decreases as grain size increases. So we can assume that the activation enthalpy is dependent on grain size. The relationship between the activation enthalpy and grain size has not been known yet. In order to obtain this relationship, β_{gj}^{-1} is expressed as a function of grain size x in the general form:

$$\beta_{gj}^{-1}=\left(\frac{\lambda}{\lambda_1}\right)_{gj}\frac{2kT}{h}\exp\left(\frac{\Delta S_{gj}^{\ddagger}}{R}\right)\cdot \exp\left[\frac{-\Delta H_{gj0}^{\ddagger}}{RT}(1+a'\ln x)\right] \qquad (15)$$

where $\Delta H_{gj0}^{\ddagger}$ represents the activation enthalpy for unit grain size, and a' is a constant. Equation (15) can be rewritten in a simple form:

$$\ln \beta_{gj}^{-1}=a\ln x+b \qquad (16)$$

where

$$a=-\frac{\Delta H_{gj0}^{\ddagger}}{RT}a',$$

and

$$b=\ln\left(\frac{\lambda}{\lambda_1}\frac{2kT}{h}e^{\Delta S^{\ddagger}/R}\right)_{gj}-\frac{\Delta H_{gj0}^{\ddagger}}{RT}$$

At a given temperature a and b are constant. Thus $\ln \beta_{gj}^{-1}$ is a linear function of $\ln x$, and the grain size dependence of β_{gj}^{-1} can be obtained from the value of a and b. An example for determining the relation between β_{gj}^{-1} and

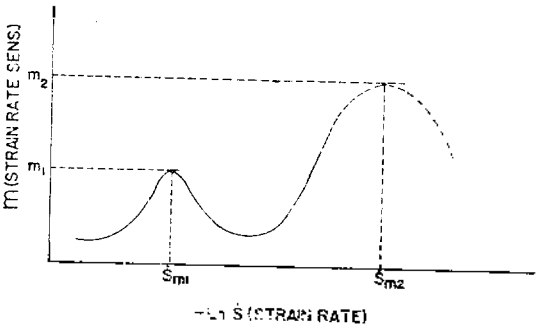

Fig. 2. Schematic plot of m (strain rate sensitivity) *vs.* $-\ln \dot{s}$(strain rate) for a system composed of two grain boundary flow units. Here the relations $\beta_{g1}<\beta_{g2}$, $\dot{s}_{m1}>\dot{s}_{m2}$ and $m1(\max.)<m2(\max.)$ hold.

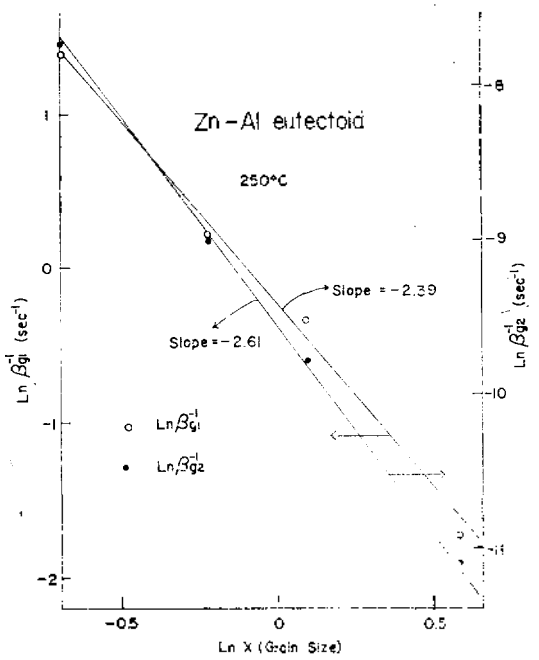

Fig. 3. Grain size dependence of $\ln \beta_{gj}^{-1}$ ($j=1$ or 2) for Zn-Al eutectoids of various grain sizes (0.5, 0.8, 1.1 and 1.8 μ) at 250 °C (experimental data from Holt[12]). The upper straight line(open circle) is referred to the left ordinate while the lower one(solid circle) to the right ordinate.

grain size is shown in *Fig.* 3, where the plot of $\ln \beta_{gj}^{-1}$ *vs.* $\ln x$ ($j=1$ or 2) are shown for Zn-Al eutectoid of fine grain size. The straight lines were obtained by a least square fit, and constants a and b were obtained from the slope and the intercept, respectively.

APPLICATIONS

1. Zn-Al Eutectoid

Mohamed and Langdon[10] prepared Zn-Al eutectoid alloys of different grain sizes by controlling the annealing time at 533°K. The experimental data of tensile test for the sample (super-Z 200) at 503°K were plotted in *Fig.* 4. From the curves of f *vs.* $-\ln \dot{s}$ the flow parameters were obtained by using the Kim-Ree method,[7] and the results are shown in *Table* 1. The β_{gj} values for different grain sizes in *Table* 1 were calculated from Eq. (16) by using the values of a (slope) and b (intercept) listed in *Table* 4 which will appear later. The method for determining a and b has been already explained in the Theory. The solid flow curves in *Fig.* 4 for different grain sizes were calculated from Eq. (5a) with the flow parameters in *Table* 1. From *Fig.* 4, one notes that the agreement between theory and experiment is very good. The results of double shear test by Mohamed *et al.*[10] for samples of various grain sizes were also analysed by using Eq. (5a), and we obtained the theoretical flow curves which agree very well with experiment, but the results are omitted here. Mohamed and Langdon[11] also studied the flow behavior for tension at different temperatures with an Instron testing machine for the Zn-Al eutectoid alloys of grain size 2.5μ prepared by Mohamed *et al.*[10] The experimental results were also in good agreement with the theoretical curves calculated from Eq. (5a), but the results are also omitted here.

Holt[12] investigated the flow behavior of Zn-Al eutectoid alloys of finer grain size. Compression tests were performed with an Instron machine. For this system, theoretical flow curves were calculated by using Eq. (5a). These curves were also in good agreement with experiment, but are not presented here. However,

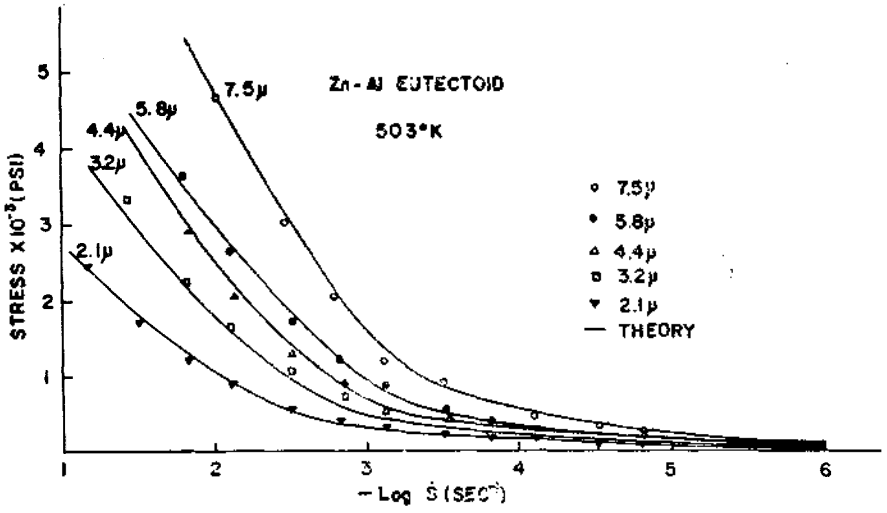

Fig. 4. Stress *vs.* -log $\dot{s}$ in tension test of Zn-Al eutectoid (Super-Z 200) with different grain sizes at 503 °K (experimental data from Mohamed *et al.*[10]).

Table 1. Flow parameters for Zn-Al eutectoids[a].

Grain size (μ)	X_{gj}/α_{gj}[b]	β_{gj}[b,c]	Temp.	Figs. and refs.
7.5	1.41×10^{3} (psi)$^{-1}$ (6.53×10) (psi)$^{-1}$	7.44×10^{2} (sec) (4.80×10^{6}) (sec)	503° K	*Fig.* 4 Mohamed *et al.*[10]
5.8	1.11×10^{3} (psi)$^{-1}$ (4.41×10) (psi)$^{-1}$	4.89×10^{2} (sec) (4.04×10^{6}) (sec)		
4.4	1.15×10^{3} (psi)$^{-1}$ (3.85×10) (psi)$^{-1}$	3.11×10^{2} (sec) (3.36×10^{6}) (sec)		
3.2	1.01×10^{3} (psi)$^{-1}$ (3.64×10) (psi)$^{-1}$	1.84×10^{2} (sec) (2.72×10^{6}) (sec)		
2.1	8.00×10^{2} (psi)$^{-1}$ (3.16×10) (psi)$^{-1}$	9.25×10 (sec) (2.05×10^{6}) (sec)		
1.8	2.41×10^{3} (psi)$^{-1}$ (1.28×10^{2}) (psi)$^{-1}$	5.20 (sec) (6.59×10^{4}) (sec)	250° C	*Fig.* 3 Holt[12]
1.1	2.70×10^{3} (psi)$^{-1}$ (1.26×10^{2}) (psi)$^{-1}$	1.60 (sec) (1.82×10^{4}) (sec)		
0.8	2.87×10^{3} (psi)$^{-1}$ (1.09×10^{2}) (psi)$^{-1}$	7.50×10^{-1} (sec) (7.92×10^{3}) (sec)		
0.5	2.56×10^{3} (psi)$^{-1}$ (1.40×10^{2}) (psi)$^{-1}$	2.44×10^{-1} (sec) (2.32×10^{3}) (sec)		
0.55	4.01×10 (MN/m^2)$^{-1}$ (2.14×10) (MN/m^2)$^{-1}$	1.63 (min) (1.40×10^{3}) (min)	20° C	*Fig.* 5 Naziri *et al.*[13]
	5.20×10 (MN/m^2)$^{-1}$ (1.20×10) (MN/m^2)$^{-1}$	1.16 (min) (1.16×10^{3}) (min)	50° C	
	2.89×10 (MN/m^2)$^{-1}$ (5.37) (MN/m^2)$^{-1}$	7.38×10^{-1} (min) (9.11×10^{2}) (min)	100° C	
	2.07×10 (MN/m^2)$^{-1}$ (2.32) (MN/m^2)$^{-1}$	5.23×10^{-1} (min) (7.55×10^{2}) (min)	150° C	
	1.40×10 (MN/m^2)$^{-1}$ (1.06) (MN/m^2)$^{-1}$	3.33×10^{-1} (min) (6.52×10^{2}) (min)	200° C	
	9.67 (MN/m^2)$^{-1}$ (5.10×10^{-1}) (MN/m^2)$^{-1}$	3.20×10^{-1} (min) (5.78×10^{2}) (min)	250° C	

[a] Unparenthesized parametric values represent the values for flow unit $g1$ and parenthesized ones for flow unit $g2$.
[b] The subscript j indicates flow unit 1 or 2.
[c] β_{gj} values for different grain sizes were obtained by introducing constants a and b in *Table* 4 to Eq. (16), and β_{gj} values for different temperatures were obtained by introducing ΔH_{gj}^{*} and A_{gj} in *Table* 5 to Eq. (14).

the β_{gj} values obtained experimentally were plotted against $\ln x$ (grain size) in *Fig.* 3 as an example for determining the constants a and b in Eq. (16). The parameters for the flow curves are shown in *Table* 1, where the β_{gj} values for various grain sizes were calculated

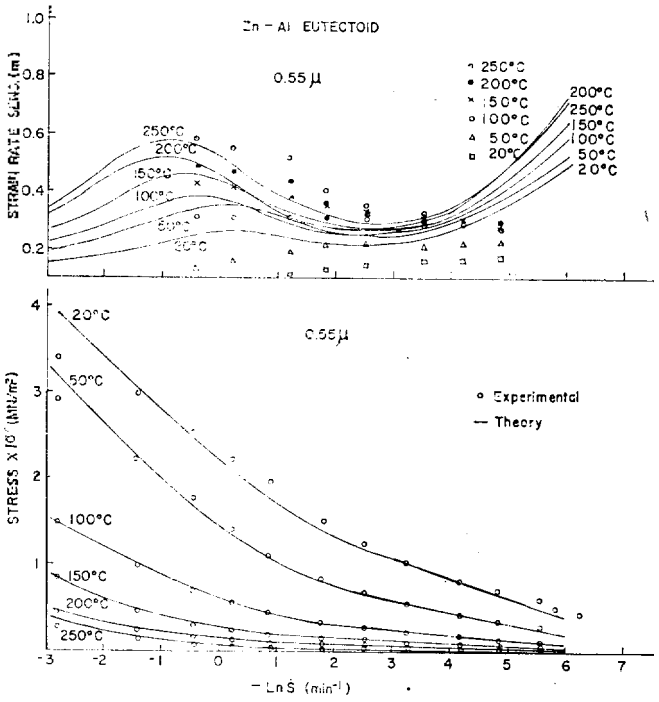

Fig. 5. Stress (lower curves) and strain rate sensitivity (upper curves) *vs.* -ln ṡ in tension test of Zn-Al eutectoids with grain size 0.55 μ at different temperatures (experimental data from Naziri[13]).

from Eq. (16) by using a and b in *Table* 4. Holt[12] also confirmed that the major contribution to the total shear at intermediate strain rates is the grain boundary sliding by observing the displacement of a surface marker.

Naziri, Pearce and Brown[13] explained mechanism of superplasticity by observing the microstructure and time-dependent flow behavior of Zn-Al eutectoids. The samples were prepared by the same method as Holt,[12] and tested by a single tension method. The experimental results from 20 to 250 °C are plotted as curves of f *vs.* -ln ṡ in the lower half of *Fig.* 5. The solid lines are the theoretical curves calculated from Eq. (5a) by introducing the flow parameters in *Table* 1. The β_{gj} values at different temperatures were calculated from Eq. (14) by using the ΔH_{gj}^* and A_{gj} values which were determined by the method previously mentioned, and are listed in *Table* 5 which will appear later. One notes from *Fig.* 5 that the agreement between theory and experiment is excellent.

The strain rate sensitivity curves for the Zn-Al eutectoid are shown in the upper half of *Fig.* 5 where experimental m (strain rate sensitivity) values were calculated from Eq. (6) by using the experimental data of f and ṡ, and the theoretical values of m were calculated from Eq. (8) by using the parametric values of X_{gj}/α_{gj} and β_{gj} given in *Table* 1. These curves are not in good agreement with experiment, but they show a similar tendency with experiment, that is, the maximum of the strain rate sensitivity curve shifts to higher ṡ with temperature in accordance with Eq. (13), and the strain rate sensitivity m also increases with temperature in agreement with Eq. (12). [Note that β_{gj} in Eqs. (12) and (13) is a function of T by Eq. (10).]. The sensitivity curve showed a tendency to have another maximum at lower ṡ, which is theoretically anticipated; in this region, however, there are no experimental data. It is reported that, in general, there appears Newtonian flow in the region of low strain rates below 10^{-7} sec^{-1}.[11] This fact is also in accord with the authors' theory according to which the sensitivity maximum with a higher value of m like Newtonian flow (m=1) appears at lower ṡ.

According to a 1 Mev/in situ electron microscopic study[13] of a sample of Zn-Al eutectoid alloy after tension, grain boundary sliding was

Table 2. Flow parameters for Pb-Sn eutectics[a].

Grain size	X_{gj}/α_{gj}[b]	β_{gj}[b,c] (sec)	Temp.	*Figs.* and refs.
(Cast) 0.92×10^{-4} in	(5.44×10^{-1}) (ksi)$^{-1}$	(8.86×10^{6})	Rm. Temp.	*Fig.* 6 Avery *et al.*[14]
0.97×10^{-4} in.	8.03×10^{-1} (ksi)$^{-1}$ (5.43×10^{-1}) (ksi)$^{-1}$	1.21×10^{3} (1.83×10^{4})		
1.10×10^{-4} in.	8.00×10^{-1} (ksi)$^{-1}$ (5.14×10^{-1}) (ksi)$^{-1}$	1.49×10^{3} (2.30×10^{4})		
1.30×10^{-4} in.	5.21×10^{-1} (ksi)$^{-1}$ (6.37×10^{-1}) (ksi)$^{-1}$	1.94×10^{3} (3.13×10^{4})		
1.70×10^{-4} in.	$[7.04\times10^{-1}]$ (ksi)$^{-1}$ 9.02×10^{-1} (ksi)$^{-1}$ (7.65×10^{-1}) (ksi)$^{-1}$	$[3.64\times10^{5}]$ 2.98×10^{3} (5.11×10^{4})		
2.60×10^{-4} in.	$[5.82\times10^{-1}]$ (ksi)$^{-1}$ 1.23 (ksi)$^{-1}$ (6.34×10^{-1}) (ksi)$^{-1}$	$[1.94\times10^{6}]$ 5.88×10^{3} (1.11×10^{5})		
5.8 μ	6.34×10^{-1} (MN/m^2)$^{-1}$ (1.25×10^{-2}) (MN/m^2)$^{-1}$	6.82×10^{2} (4.73×10^{6})	422°K	*Fig.* 7 Mohamed *et al.*[15]
	1.03 (MN/m^2)$^{-1}$ (1.81×10^{-2}) (MN/m^2)$^{-1}$	9.53×10^{2} (7.28×10^{6})	392°K	
	1.89 (MN/m^2)$^{-1}$ (2.82×10^{-2}) (MN/m^2)$^{-1}$	1.43×10^{3} (1.22×10^{7})	361°K	
	2.91 (MN/m^2)$^{-1}$ (6.90×10^{-2}) (MN/m^2)$^{-1}$	2.09×10^{3} (1.99×10^{7})	336°K	

[a] Unparenthesized parametric values represent the values for flow unit $g1$, parenthesized ones for flow unit $g2$, and square bracketed ones for flow unit $d1$.

[b] The subscript j indicates flow unit 1 or 2.

[c] β_{gj} values for different grain sizes were calculated by introducing constants a and b in *Table* 4 to Eq. (16), and the β_{gj} values for different temperatures were obtained by introducing $\Delta H_{\epsilon j}^{*}$ and $A_{\epsilon j}$ in *Table* 5 to Eq. (14).

mainly observed at interphase boundaries, and the pinching-off of α-grains (Al-rich phase) by β-grains (Zn-rich phase) were also found. Dislocation activities were also observed to some extent in α-phase, but not in β-phase. These experimental observations and flow data, support our theory on the flow of Zn-Al eutectoids.

2. Pb-Sn Eutectic

Avery and Backofen[14] investigated the microscopic structure, and tested mechanical properties of Pb-Sn eutectics to study the superplasticity. Test samples of different metallographic mean free paths were prepared by controlling annealing temperatures (room temperature, 100 and 150 °C) and annealing time of a Pb-Sn eutectic cast extruded at 298 °K. The experimental results are shown in the lower half of *Fig.* 6. The solid curves were theoretically calculated from Eq. (5a) by using the parameters in *Table* 2 except for the curves of grain size 1.7×10^{-4} and 2.6×10^{-4} in., for the latter two curves Eq. (2a) was used (see below). Referring to *Fig.* 6, the cast sample (grain size: 0.92×10^{-4} in.) deforms with only one

kind of flow unit ($g1$) at higher stress levels than any other annealed samples, inspite of the finest grain size of the sample. Annealed samples having the grain sizes from 0.97×10^{-4} to 1.3×10^{-4} in. show flow curves due to two kinds of flow units ($g1$ and $g2$) connected in parallel. For the samples of grain sizes above 1.7×10^{-4} in., however, an additional flow unit of dislocation movement ($d1$) appears at higher stress levels, the $d1$ unit being connected in series with the aforementioned $g1$ and $g2$ flow units, *i.e.*, this case corresponds to Kim-Ree's Case 4.[7] Consequently, the flow curves for grains of 1.7×10^{-4} and 2.6×10^{-4} in. were calculated from Eq. (2a) where $i=1$, $j=2$ and $f_{d1}=f$. The flow parameters of the samples are shown in *Table* 2, and β_{gj} values for different grain sizes were calculated by introducing the values of a and b in *Table* 5 into Eq. (16).

The strain rate sensitivity curves corresponding to all the flow curves are shown at the upper half of *Fig.* 6, and are compared with experiment. In the calculation of the theoretical m curves, the contribution of dislocation movement for curves of grain size 1.7×10^{-4} and 2.6×10^{-4} in. were neglected. One notes from *Fig.* 6 that the cast specimen has no superplastic region at all, while the annealed specimens are superplastic below certain $\dot{s}$. One also notes that the maxima of the sensitivity curves are not sharp in this case, and that the maximum m values have tendency to increase and

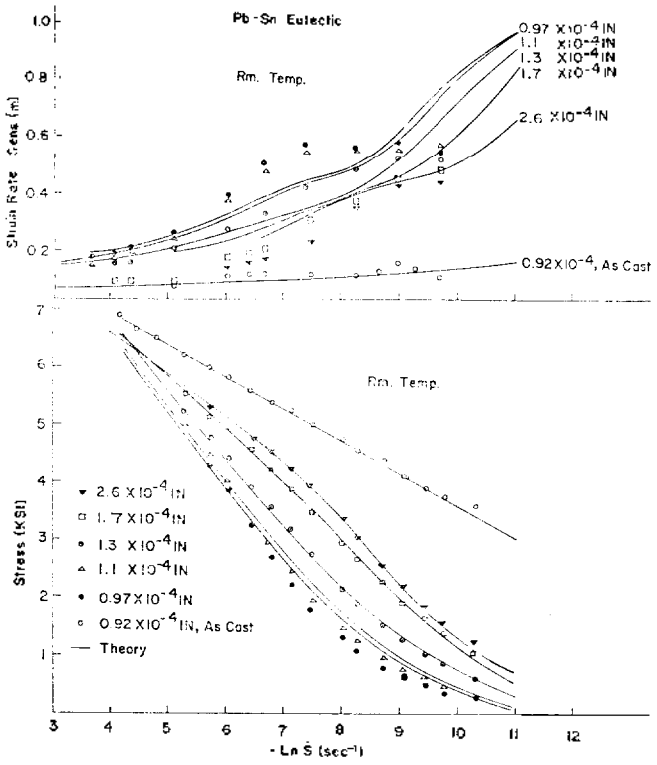

Fig. 6. Stress (lower curves) and strain rate sensitivity (upper curves) *vs.* $-\ln\dot{s}$ in tension test of Pb-Sn eutectic with different grain sizes at room temperature (experimental data from Avery[14]).

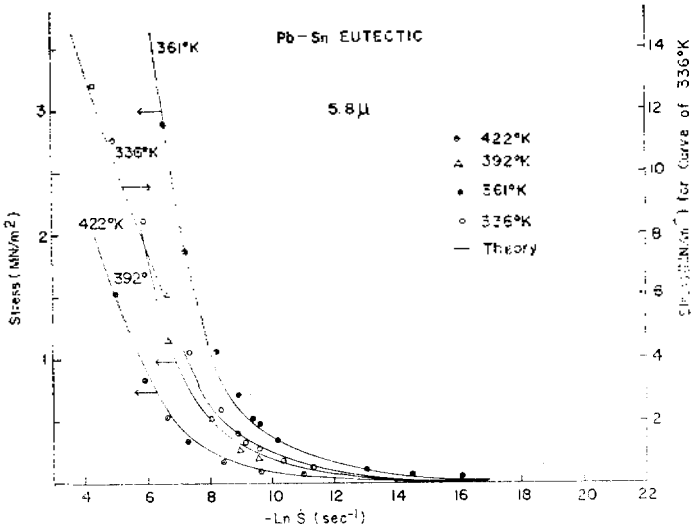

Fig. 7. Stress *vs.* $-\ln\dot{s}$ in double shear test of Pb-Sn eutectics over the range of 336 to 422 °K with grain size 5.8μ (experimental data from Mohamed[15]). The curve at 336 °K is referred to the right ordinate while the other curves to the left ordinate.

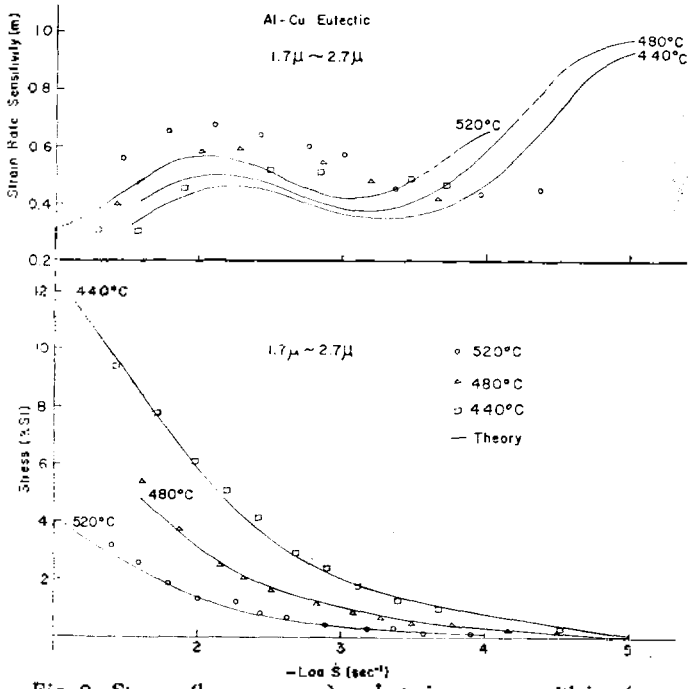

Fig. 8. Stress (lower curves) and strain rate sensitivity (upper curves) *vs.* -log ṡ in tension test of Al-Cu eutectics over the range of 440 to 520 °C with grain size 1.7 to 2.7 μ (experimental data from Holt[17]).

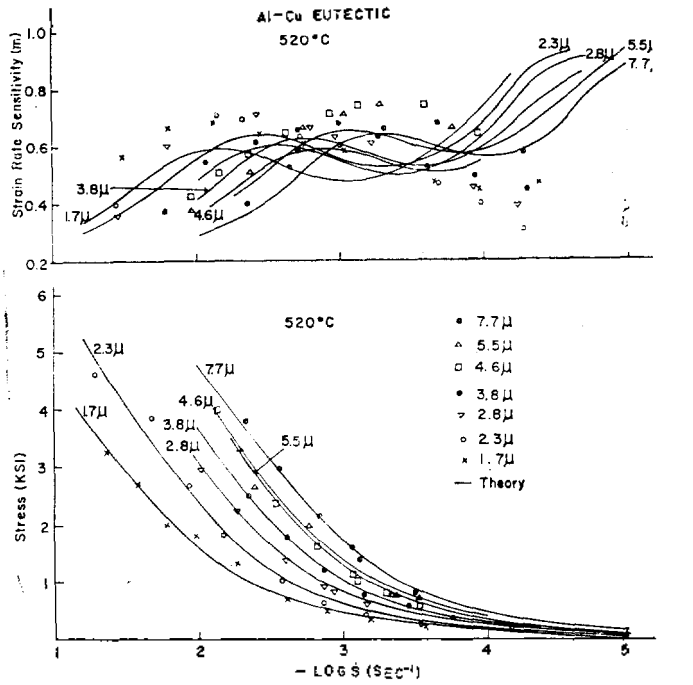

Fig. 9. Stress (lower curves) and strain rate sensitivity (upper curves) *vs.* -log ṡ in tension test of Al-Cu eutectics with different grain sizes at 520 °C (experimental data from Holt[17]).

appear at higher ṡ as the grain size decreases. These experimental facts are also found in the theoretical curves. [Refer to Eqs. (12) and (13) where β_{gl} is a function of grain size x by Eq. (16).] The special behavior of the cast specimen, which shows no superplasticity inspite of its fine grain size, is considered to be due to its rod-like shape, that is, strongly asymmetric grain shape.

Mohamed and Langdon[15] investigated the creep behavior of superplastic Pb-Sn eutectics over the range of grain size from 5.8 to 14.5 μ at temperatures from 336 to 422 °K. The chemical composition of the specimen was 38.1 wt. % Pb, 61.9 wt. % Sn and ppm order of impurities. Mechanical tests were performed under double shear condition. Experimental results at different temperatures are shown in *Fig.* 7. The solid curves are calculated theoretically from Eq. (5a). The flow parameters are tabulated in *Table* 2 where β_{gj} values were calculated by introducing ΔH_{gj}^{*} and A_{gj} in *Table* 5 into Eq. (14). The theoretical flow curves are in good agreement with experiment (see *Fig.* 7).

Martin and Backofen[16] investigated superplasticity of different grain sizes for two kinds of electroplated composites of Pb and Sn, one of them is an as-plated and the other is an annealed sample. The experimental results of tension test with an Instron were in good agreement with our theory [Eq. (5a)]. (The results are not shown here.) Martin *et al.*[16]

Table 3. Flow parameters for some eutectic alloys[a].

Alloys	Grain size(μ)	X_{gj}/α_{gj}[b]	β_{gj}[b,c]	Temp. (°C)	*Figs.* and refs.
Al-Cu eutectic	1.7	1.23 (ksi)$^{-1}$ (1.05×10^{-1}) (ksi)$^{-1}$	7.66×10 (sec) (1.54×10^{4}) (sec)	520	*Fig.* 8 Holt *et al.*[17]
		1.93 (ksi)$^{-1}$ (2.26×10^{-1}) (ksi)$^{-1}$	1.08×10^{2} (sec) (2.49×10^{4}) (sec)	480	
		2.65 (ksi)$^{-1}$ (3.91×10^{-1}) (ksi)$^{-1}$	1.58×10^{2} (sec) (4.24×10^{4}) (sec)	440	
	7.7	1.28 (ksi)$^{-1}$ (9.98×10^{-2}) (ksi)$^{-1}$	1.12×10^{3} (sec) (8.15×10^{4}) (sec)	520	*Fig.* 9 Holt *et al.*[17]
	5.5	1.39 (ksi)$^{-1}$ (9.65×10^{-2}) (ksi)$^{-1}$	6.43×10^{2} (sec) (5.50×10^{4}) (sec)		
	4.6	1.52 (ksi)$^{-1}$ (1.48×10^{-1}) (ksi)$^{-1}$	4.80×10^{2} (sec) (4.46×10^{4}) (sec)		
	3.8	1.50 (ksi)$^{-1}$ (1.13×10^{-1}) (ksi)$^{-1}$	3.50×10^{2} (sec) (3.57×10^{4}) (sec)		
	2.8	1.55 (ksi)$^{-1}$ (1.25×10^{-1}) (ksi)$^{-1}$	2.13×10^{-2} (sec) (2.50×10^{4}) (sec)		
	2.3	1.52 (ksi)$^{-1}$ (9.31×10^{-2}) (ksi)$^{-1}$	1.54×10^{2} (sec) (1.98×10^{4}) (sec)		
	1.7	1.25 (ksi)$^{-1}$ (1.03×10^{-1}) (ksi)$^{-1}$	9.37×10 (sec) (1.39×10^{4}) (sec)		
Mg-Al eutectic	2.2	6.92×10^{3} (psi)$^{-1}$ (2.07×10^{2}) (psi)$^{-1}$	4.29 (min) (3.77×10^{5}) (min)	250	*Fig.* 10 D. Lee[18]
		3.54×10^{3} (psi)$^{-1}$ (8.68×10) (psi)$^{-1}$	1.68 (min) (1.25×10^{5}) (min)	300	
		3.72×10^{3} (psi)$^{-1}$ (3.56×10) (psi)$^{-1}$	7.67×10^{-1} (min) (4.92×10^{4}) (min)	350	
		3.40×10^{3} (psi)$^{-1}$ (2.37×10) (psi)$^{-1}$	3.93×10^{-1} (min) (2.24×10^{4}) (min)	400	
Sn-5% Bi eutectic	1.2	4.66×10^{3} (psi)$^{-1}$ (1.20×10^{2}) (psi)$^{-1}$	3.96 (min) (2.06×10^{3}) (min)	Rm. Temp.	*Fig.* 11 Alden[19]
	2.3	3.38×10^{3} (psi)$^{-1}$ (1.54×10^{2}) (psi)$^{-1}$	3.50×10 (min) (8.90×10^{3}) (min)		
	3.5	[9.62×10^{2}] (psi)$^{-1}$ 3.71×10^{3} (psi)$^{-1}$ (1.43×10^{2}) (psi)$^{-1}$	[4.66×10^{4}] (min) 1.42×10^{2} (min) (2.33×10^{4}) (min)		
	5.5	[1.56×10^{3}] (psi)$^{-1}$ 2.54×10^{3} (psi)$^{-1}$ (1.74×10^{2}) (psi)$^{-1}$	[7.44×10^{7}] (min) 5.91×10^{2} (min) (6.34×10^{4}) (min)		

Table 3. continued

[a] Unparenthesized parametric values represent the values for flow unit $g1$, parenthesized ones for flow unit $g2$, and square bracketed ones for flow unit $d1$.

[b] The subscript j indicates flow unit 1 or 2.

[c] $\hat{\beta}_{ij}$ values for different grain sizes were calculated by introducing constants a and b in *Table* 4 to Eq. (16), and the β_{ij} values for different temperatures were calculated by introducing ΔH_{ij}^{*} and A_{ij} in *Table* 5 to Eq. (14).

Table 4. Grain size dependence of ln β_{ij}^{-1} (ln $\beta_{ij}^{-1}=a$ ln $x+b$)[a].

Eutectic or eutectoids	a	b	Temp.	Flow unit	*Figures*
Zn-Al eutectoid[b]	−1.64	− 3.31	503 °K	$g1$	*Fig.* 4
	−0.667	−14.04		$g2$	
	−2.39	− 0.245	250 °C	$g1$	*Fig.* 3
	−2.61	− 9.56		$g2$	
Pb-Sn eutectic[c]	−1.60	− 7.15	Rm. Temp.	$g1$	*Fig.* 6
	−1.83	− 9.87		$g2$	
Al-Cu eutectic[d]	−1.64	− 3.67	520 °C	$g1$	*Fig.* 9
	−1.17	− 8.92		$g2$	
Sn-Bi eutectic	−3.35	− 0.765	Rm. Temp.	$g1$	*Fig.* 11
	−2.25	− 7.22		$g2$	

[a] Here a (slope) and b (intercept) were obtained from the plot of ln β_{ij}^{-1} *vs.* ln x (grain size), and by using least square method (see *Fig.* 3).

[b] The a and b values were also obtained by applying our method to Mohamed *et al.*'s data (463 °K) for the system of Zn-Al eutectoid,[10] and to J. D. Lee *etal.*'s data (204 °C) for the system of Zn-0.1Ni-0.04 Mg.[21] However, the results have been omitted.

[c] Our method was applied to Mohamed *et al*'s data (422 °K) for the system of Pb-Sn eutectic[15] and Martin *et al.*'s data (room temp.) for the system of Pb-Sn composites electroplated,[16] and for the latter system annealed at 100 or 150° C.[16] The a and b values obtained, however, are not shown here.

[d] D. Lee's data (400 °C) for the Mg-Al eutectic[18] were treated by our method. But the a and b values obtained have been omitted here.

expected that the as-plated and annealed specimens would show different patterns of flow curves because of the different grain boundary structures. But experiments showed similar results for the two specimens, and superplastic ranges were also similar. Thus grain boundary structure may not be the key factor for superplasticity in this case.

3. Al-Cu Eutectic

Holt and Backofen[17] investigated the mechanical properties of Al-Cu eutectic alloys for different grain sizes at various temperatures in relation to superplasticity. An Instron machine was used to test the mechanical properties. The results of mechanical test at different temperatures are plotted in the lower half of *Fig.* 8, and those for different grain sizes in the lower half of *Fig.* 9. The solid curves are theoretical ones calculated from Eq. (5a) by using the flow parameters in *Table* 3. The β_{gj} values for various grain sizes in *Table* 3 were calculated from Eq. (16) by introducing constants a and b in *Table* 4, and those for different temperatures from Eq. (14) by using ΔH_{ij}^{*} and A_{gj} values in *Table* 5. The theoretical flow curves are in good agreement with experiment. One sees that the flow curves in *Figs.* 8 and 9 behave in a similar way as in the cases of Pb-Sn eutectics

and Zn-Al eutectoids for temperature and grain size changes.

The strain rate sensitivity curves corresponding to the flow curves in the lower halves of *Figs.* 8 and 9 were calculated using Eq. (8), and are shown in the upper halves of *Fig.* 8 and *Fig.* 9, respectively, and are compared with experiment. The strain-rate sensitivity curves show that Al-Cu eutectics are superplastic in the whole range of $\dot{s}$, and show that the sensitivity curves also similarly behave as in the cases of Pb-Sn eutectics and Zn-Al eutectoids.

According to a microstructural observation on the Al-Cu eutectic, the grain boundary migration and recrystallization rate were increased prominently by straining. The Al-Cu eutectics are binary alloys of two phases, κ-Al and $CuAl_2$. Considering that the grain boundary movement is the major contribution to the total deformation, our assumption concerning the movement by two grain boundary flow units for Al-Cu eutectics is considered to be reasonable.

4. Mg-Al Eutectic

D. Lee[18] investigated superplastic phenomena of Mg-Al eutectics by measuring mechanical properties, and by comparing them with the microstructural observations at different temperatures and grain sizes. The ideal composition of Mg-Al eutectics is $Mg_{27}Al_{12}$, but composition of test specimens were 66.8 ± 0.3 wt. % of Mg (eutectic composition of Mg is 67.7 wt. %) and 33.6 ± 0.3 wt. % of Al. In order to obtain the specimens of different grain sizes, the ingots of the eutectic were heated at 400 °C under He atmosphere for different duration of time and quenched into water. An Instron was used as a test machine, and TEM (transmission electron microscopy) and SEM (scanning electron microscopy) were used to observe the metallographic structures. The experimental values of f and $\dot{s}$ of the Mg-Al eutectics at different temperatures are plotted in *Fig.* 10. The Mg-Al eutectics are binary and two phase alloys composed of δ- and γ-phases. So the deformation of the eutectics are considered to flow by a mechanism

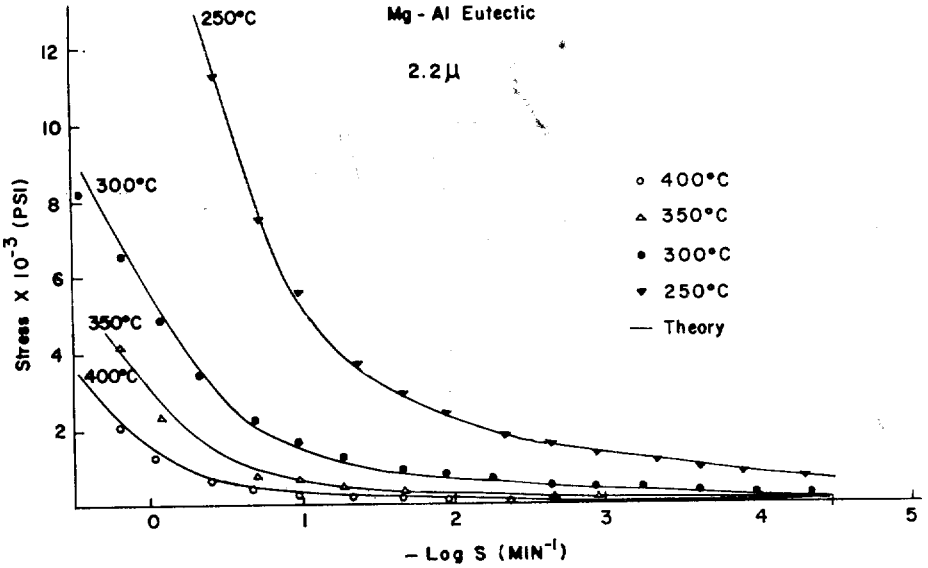

Fig. 10. Stress *vs.* -log $\dot{s}$ over the range of 250 to 400 °C for Mg-Al eutectic alloy with grain size 2.2μ (experimental data from D. Lee[18]).

with two grain boundary flow units. Under this assumption the solid curves in *Fig.* 10 were calculated from Eq. (5a) by introducing flow papameters in *Table* 3. The parameters β_{gj} at different temperatures for the Mg-Al eutectics in *Table* 3 were calculated from Eq. (14) by introducing ΔH_g^* and A_{gj} in *Table* 5. The theoretical flow curves in *Fig.* 10 are in good agreement with experiment. The theoretical flow curves for the Mg-Al eutectics of different grain sizes at 400 °C were calculated from Eq. (5a) with good results, but they are omitted here.

According to the surface observation with the SEM[18] for the Mg-Al eutectic after deformation, grain boundary shear, grain rotation and grain boundary migration occurred in the low to middle ranges of shear rates; and according to the TEM examination of internal structure, the evidence of dislocation traces was not observed in a whole range of strain rates. But D. Lee observed by TEM that in a higher strain-rate range, dislocation traces began to appear. According to our results of analysis of D. Lee's experiment,[18] however, the contribution of dislocation flow to the total deformation was negligibly small so that it was unable to detect its contribution.

5. Sn-Bi Eutectic

In order to study plastic deformation processes of Sn-5% Bi eutectics which has no metastability, Alden[19] investigated the mechanical properties and microstructure of the alloy. The specimens were prepared by a special process, and were subjected to a tension test by an Instron machine at $T/Tm=0.6$, where Tm is the melting temperature in Kelvin scale. Referring to the phase diagram of the Sn-Bi system,[20] Sn dissolves about 1 wt. % Bi at room temperature, and the remaining 4 % is present as essentially pure Bi.

The results of tension test with an Instron are plotted in *Fig.* 11. The experiment shows some pattern different from usual eutectic or eutectoid alloys. That is, specimens of smaller grain sizes (1.2 and 2.3 μ) present the normal flow curves which can be expressed by Eq. (5a), whereas the flow curves for larger grain sizes

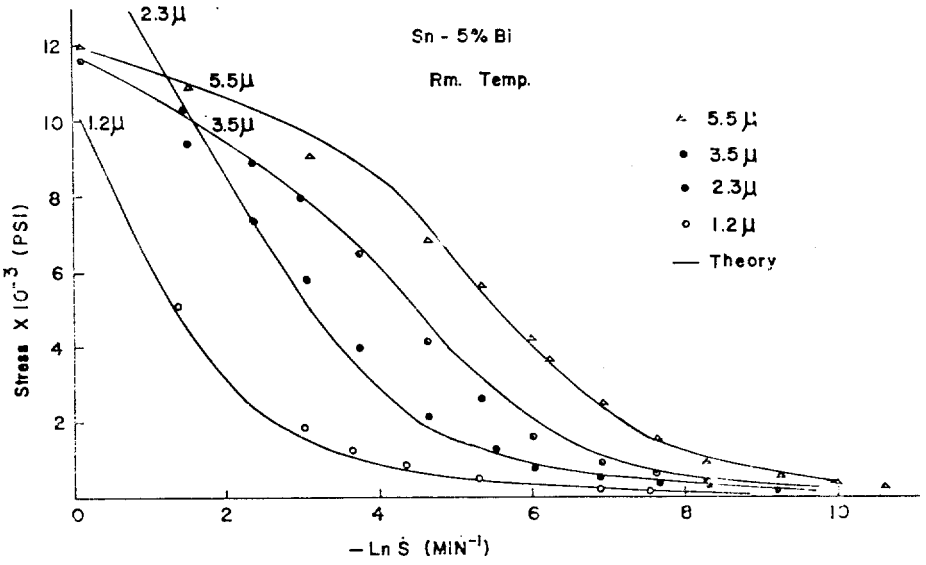

Fig. 11. Stress *vs.* -ln $\dot{s}$ in tension test of Sn-5% Bi with different grain sizes at room temperature (experimental data from Alden[19]).

(3.5, 5.5 μ) are expressed by three kinds of flow units, *i.e.*, flow units $g1$ and $g2$ connected in parallel and flow unit $d1$ conneted in series with the $g1$ and $g2$ system, corresponding to Kim-Ree's Case 4.[7] The solid curves in *Fig.* 11 were Calculated from Eq. (5a) for 1.2 and 2.3 μ grains, and from Eq. (2a) (with $i=1$, $j=2$ and $f_{d1}=f$) for 3.5 and 5.5 μ grains. The necessary parameters are tabulated in *Table* 3, and the β_{gj} values were calculated from Eq. (16) by using the constants a and b in *Table* 4. Note that we have already found an example corresponding to Kim-Ree's Case 4 in the Pb-Sn eutectics of grain sizes of 1.70×10^{-4} and 2.6×10^{-4} in. (see *Fig.* 6 and *Table* 2).

As a microscopical evidence of grain boundary sliding, the phenomena of grannular surface roughening, scratch-offsets, rotation, the distorted appearance of boundary region and equiaxed grain structure were observed after 1000 % elongation. Alden[19] also concluded that as the grain size increases, the slip, which is considered to be due to dislocation movement, is the high rate deformation mechanism. This was based partly on mechanical evidence and partly on induction.

Finally, J. D. Lee and Niessen[21] developed a new dispersion strengthened Zn alloy which has high yield strength at room temperature and has superplasticity at elevated temperatures. The normal composition of this alloy was Zn-0.10Ni-0.04Mg. The mechanical properties and superplasticity were tested. Our theory were also applied to this new alloy. Theory and experiment were in good agreement, but the detailed explanation of the results are omitted here.

DISCUSSIONS

1. Activation Enthalpies for Grain Boundary Flow

In the theory, it has been mentioned that two kinds of activation enthalpies (ΔH_{g1}^* and ΔH_{g2}^*) are expected in the superplastic deformation of eutectic or eutectoid alloys, ΔH_{g1}^* and ΔH_{g2}^* being equal to the activation enthalpies for self-diffusion of two kinds of atoms. Applying Eq. (14), we obtained the activation enthalpies from the slopes of the plots of $\ln\{\beta_T^-\}$ *vs.* $1/T$. The values for various eutectics and eutectoids are tabulated in *Table* 5.

First consider the case of Zn-Al eutectoids. The activation enthalpies for flow units $g1$ and $g2$ are found to be $\Delta H_{g1}^*=2.16$ and $\Delta H_{g2}^*=1.17$ kcal/g·atom for the sample of 0.55 μ grain size, and $\Delta H_{g1}^*=10.8$ and $\Delta H_{g2}^*=4.6$ kcal/g·atom for the sample of 2.5 μ grain size. We note from *Table* 5 that the activation enthalpies increase as the grain size increases in agreement with the anticipation from Eq. (16). [Note that a and b in Eq. (16) are negative, see *Table* 4.] The activation energy for self-diffusion of a bicrystal of pure Al is twice as large as that of pure Zn (see *Table* 5). Taking this into account, the values of ΔH_{g1}^* (2.16 kcal/g·atom for 0.55 μ and 10.8 kcal/g·atom for 2.5 μ) may be assigned to the activation enthalpies of Al, and those of ΔH_{g2}^* (1.17 kcal/g·atom for 0.55 μ and 4.6 kcal/g·atom for 2.5 μ) to the enthalpies of Zn. On the other hand, Naziri *et al.*[13] obtained ΔH_g^* values different from ours. The reason for this difference will be discussed in a later paper.

Next we consider the case for Pb-Sn eutectic alloys. There are many literature values for the activation enthalpy for Pb-Sn eutectics, such as 11.5,[26,27] 10.5 to 17.9,[28] 7.9,[29] 12.9,[30] and 9.32 kcal/g. atom,[31] but the grain sizes of the samples have not been specified. We consider that the spread of the values are due to the different grain sizes. Our values of ΔH_{gj}^* in this work, $\Delta H_{g1}^*=3.68$ and $\Delta H_{g2}^*=4.71$

Table 5. ΔH_i^* values for eutectic and eutectoid alloys[a].

Samples	Grain size	ΔH_i^*(kcal/g. atom)	A_{gj} in Eq. (14)	References
Zn-Al eutectoid	0.55 μ	2.16[ΔH_{g1}^*(Al)] 1.17[ΔH_{g2}^*(Zn)]	3.21 −5.23	This work
	2.5 μ	10.8 [ΔH_{g1}^*(Al)] 4.6 [ΔH_{g2}^*(Zn)]	9.02 −7.24	This work[b]
	4.4 μ	ca. 25(high stress) ca. 16(low stress)		Mohamed *et al.*[10]
Pure Al	Bicrystal	8.5		Tung[22]
Pure Zn	Bicrystal	4.7		Turner[23]
Pb-Sn eutectic	5.8 μ	3.68[ΔH_{g1}^*(Sn)] 4.71[ΔH_{g2}^*(Pb)]	−2.14 −9.75	This work
		7.9		Aldrich[29]
	ca. 2 μ	11.5		Cline,[26] Baudelet[27]
Pure Pb	*ca.* 1 mm	15.8[c]		Okkerse[24]
	Bicrystal	4.7[c]		Stark[32]
Pure Sn	*ca.* 0.5 mm	9.56[c]		Lange[25]
Al-Cu eutectic	1.7 to 2.7 μ	10.2[ΔH_{g1}^*(Al)] 14.2[ΔH_{g2}^*(Cu)]	2.13 −0.640	This work
Mg-Al eutectic	2.2 μ	11.2[ΔH_{g1}^*(Al)] 13.2[ΔH_{g2}^*(Mg)]	9.27 −0.614	This work
	10.6 μ	19.2[c]		D. Lee[18]
Zn-0.10Ni -0.04Mg	1.9 μ	9.63[ΔH_{g1}^*] 8.09[ΔH_{g2}^*]	7.95 0.456	This work[d]
	1.9 μ	13.1		J. D. Lee *et al.*[21]

[a] ΔH_{g1}^* and ΔH_{g2}^* represent activation enthalpies for flow units $g1$ and $g2$, respectively. The expected diffusing atoms are given in parentheses.

[b] The ΔH_{gi}^* values were determined by analysing Mohamed *et al.*'s data,[10] but the flow parameters obtained at various temperatures have been omitted in *Table* 1.

[c] These values were obtained by tracer diffusibn experiment.

[d] The ΔH_{gi}^* values were determined by analysing J. D. Lee *et al.*'s data,[21] but the obtained flow parameters X_{gj}/α_{gj} and β_{gj}, have been omitted in *Table* 3.

kcal/g·atom were calculated from Mohamed *et al.*'s data[15] using Eq. (14). But Mohamed *et al.* reported ΔH^* values different from ours. The reason for this difference will also be discussed in a later paper. Meanwhile Stark's self-diffusion data[32] for Pb-bicrystal is 4.7 kcal/g·atom which is equal to our ΔH_{g2}^*(=4.71 kcal/atom) of Pb-Sn eutectics. This fact is reasonable because the shear surface of grain boundaries of the bicrystal is nearly equal to that of the sample of 5.8 μ grain. And comparing the activation enthalpy for self-

diffusion of Pb with that of Sn, one notes the value of Pb(=15.8 kcal/g. atom) for *ca.* 1 mm grain sized sample is greater than that of Sn (=9.56 kcal/g·atom) for *ca.* 0.5 mm grain sized sample (refer to *Table* 5). So ΔH_{g1}^*(=3.68 kcal /g·atom) may be assigned to the activation enthalpy of Sn and ΔH_{g2}^* (=4.71 kcal/g. atom) to that of Pb.

For the case of Al-Cu eutectic alloy, we obtained the two activation enthalpies ΔH_{g1}^*= 10.2 and ΔH_{g2}^*=14.2 kcal/g·atom (see *Table* 5). Since ΔH_{g1}^* of Al-Cu eutectics of 1.7 to 2.7 μ grain size is similar in magnitude to the activation enthalpy(=10.8 kcal/g·atom) of Al of Zn-Al eutectoids of 2.5 μ grain size, the ΔH_{g1}^* for Al-Cu eutectics could be assigned to that for Al self-diffusion and ΔH_{g2}^* to that for Cu self-diffusion.

For Mg-Al eutectic alloys, D. Lee[18] reported the activation enthalpy (19.2 kcal/g·atom) for grain boundary diffusion creep. On the other hand, we obained from D. Lee's creep data[18] the values of ΔH_{g1}^*=11.2 and ΔH_{g2}^*=13.2 kcal /g·atom (see *Table* 5). Since D. Lee's value of 19.2 kcal/g·atom is the activation enthalpy for the sample of grain size 10.6 μ, the value for 2.2 μ sample would be smaller than this. The authors' value ΔH_{g1}^*=11.2 kcal/g·atom for Mg-Al eutectic (2.2 μ) is nearly equal to that of Al(=10.8 kcal/g·atom) in Zn-Al eutectoids of similar grain size (2.5 μ), so our value of ΔH_{g1}^* =11.2 kcal/g·atom for Mg-Al eutectics is considered to be the values for Al self-diffusion, and ΔH_{g2}^*=13.2 kcal/g·atom to be that for Mg self-diffusion.

For the Zn-0.10 Ni-0.04 Mg alloy, the activation enthalpies were calculated as ΔH_{g1}^*= 9.63 kcal/g. atom and ΔH_{g2}^*=8.09 kcal/g·atom which were obtained from J. D. Lee *et al.*'s experimental data[21] by using Eq. (14). On the other hand, J. D. Lee *et al.* obtained ΔH_f^*=13.1 kcal/g. atom from the same experimental data.[21] Since there is no literature value for self-diffusion of Ni and Mg, it is difficult to assign our ΔH_{gi}^* values to the components for this system.

ACKNOWLEDGEMENT

The authors express their appreciations to Korea Research Center for Theoretical Physics and Chemistry and to Euisok Research Foundation for financial support of this research.

REFERENCES

1. C.F. Pearson, *J. Inst. Metals*, **54**, 111 (1934).
2. E.E. Underwood, *J. Metals*, **14**, 914 (1962).
3. W. A. Backofen, I. R. Turner and D. H. Avery, *Trans. Quart. A.S.M.*, **57**, 980 (1964).
4. T.H. Alden, *J. Aust. Inst. Metals*, **14**, 207 (1969).
5. R. C. Gifkins and K. U. Snowden, *Trans. Met. Soc. AIME*, **239**, 910 (1967).
6. M. F. Ashby and R. A. Verrall, *Acta Met.*, **21**, 149 (1973).
7. C. H. Kim and T. Ree, *J. Korean Chem. Soc*, **21**, 330 (1977).
8. H. Eyring, *J. Chem. Phys.*, 4, 283 (1936).
9. G.E. Dieter, "Mechanical Metallurgy", 2nd Ed., McGraw-Hill Book Co., Inc., New York, 1976.
10. F.A. Mohamed and T.G. Langdon, *Acta Met.*, **23**, 117 (1975).
11. F. A. Mohamed, M.M.I. Ahmed and T. G. Langdon, *Met. Trans.*, **8A**, 933 (1977).
12. D. L. Holt, *Trans. Met. Soc. AIME*, **242**, 25 (1968).
13. H. Naziri, R. Pearce, M. Henderson Brown and K.F. Hale, *Acta Met.*, **23**, 489 (1975).
14. D.H. Avery and W.A. Backofen, *Trans. ASM.*, **58**, 551 (1965).
15. F.A. Mohamed and T.G. Langdon, *Phil. Mag.*, **32**, 697 (1975).
16. P.J. Martin and W.A. Backofen, *Trans. ASM.*, **60**, 352 (1967).
17. D.L. Holt and W.A. Backofen, *Trans. ASM.*,

59, 755 (1966).
18. D. Lee, *Acta Met.*, **17**, 1057 (1969).
19. T.H. Alden, *Acta Met.*, **15**, 469 (1967).
20. M. Hansen, "Constitution of Binary Alloys," McGraw-Hill, New York, 1958.
21. J.D. Lee and P. Niessen, *Met. Trans.*, **4**, 949 (1973).
22. S. K. Tung and R. Maddin, *Trans. AIME*, **209**, 905 (1957).
23. P. A. Turner, Ph. D. Thesis, University of London, 1965.
24. B. Okkerse, *Acta Met.*, **2**, 551 (1954).
25. W. Lange and D. Bergner, *Phys. Stat. Sol.*, **2**, 1410 (1962).
26. H. E. Cline and T. H. Alden, *Trans. Met. Soc. AIME*, **239**, 710 (1967).
27. B. Baudelet and M. Suery, *J. Mater. Sci.*, **7**, 512 (1972).
28. D. H. Avery and J. M. Stuart, "Surfaces and Interfaces II: Physical and Mechanical Properties," Edited by J. J. Burke, N. L. Reed and V. Weiss, Syracuse Univ. Press, Syracuse, P.371, 1968.
29. J.W. Aldrich and D.H. Avery, "Ultrafine-grain Metals", P.397, Ed., J. J. Burke and V. Weiss, Syracuse Univ. Press, Syracuse, 1970.
30. R. H. Johnson, R. B. Jones and E. C. Sykes, *Met. Rev.*, **15**, 115 (1970).
31. R. Horiuchi, A. B. El-Sebai and M. Otsuka, *Phys. Stat. Sol.* (a), **21**, K89 (1974).
32. J. P. Stark, W. R. Upthegrove, *Trans. ASM*, **59**, 479 (1966).